Acta Oceanol. Sin., 2021, Vol. 40, No. 12, P. 135–147
https://doi.org/10.1007/s13131-021-1883-2
http://www.aosocean.com
E-mail: ocean2@hyxb.org.cn

Radial velocity of ocean surface current estimated from SAR Doppler frequency measurements—a case study of Kuroshio in the East China Sea

Lihua Wang[1, 2, 3]*, Benwei Shi[2], Yunxuan Zhou[2], Hui Sheng[2], Yanghua Gao[3], Li Fan[3], Ziheng Yang[4]

[1] Department of Geography and Spatial Information Techniques/Center for Land and Marine Spatial Utilization and Governance Research, Ningbo University, Ningbo 315211, China

[2] State Key Laboratory of Estuarine and Coastal Research, East China Normal University, Shanghai 200062, China

[3] Chongqing Institute of Meteorological Sciences, Chongqing 401147, China

[4] College of Resources and Environment, Chengdu University of Information Technology, Chengdu 610225, China

Received 8 April 2021; accepted 8 July 2021

Abstract

Ocean currents are a key element in ocean processes and in meteorology, affecting material transport and modulating climate change patterns. The Doppler frequency shift information of the synthetic aperture radar (SAR) echo signal can reflect the dynamic characteristics of the sea surface, and has become an essential sea surface dynamic remote sensing parameter. Studies have verified that the instantaneous Doppler frequency shift can realize the SAR detection of the sea surface current. However, the validation of SAR-derived ocean current data and a thorough analysis of the errors associated with them remain lacking. In this study, we derive high spatial resolution flow measurements for the Kuroshio in the East China Sea from SAR data using a theoretical model of shifts in Doppler frequency driven by ocean surface current. Global ocean multi observation (MOB) products and global surface Lagrangian drifter (GLD) data are used to validate the Kuroshio flow retrieved from the SAR data. Results show that the central flow velocity for the Kuroshio derived from the SAR is 0.4–1.5 m/s. The error distribution between SAR ocean currents and MOB products is an approximate standard normal distribution, with the 90% confidence interval concentrated between –0.1 m/s and 0.1 m/s. Comparative analysis of SAR ocean current and GLD products, the correlation coefficient is 0.803, which shows to be significant at a confidence level of 99%. The cross-validation of different ocean current dataset illustrate that the SAR radial current captures the positions and dynamics of the Kuroshio central flow and the Kuroshio Counter Current, and has the capability to monitor current velocity over a wide range of values.

Key words: Doppler frequency, radial velocity, ocean current, SAR, Kuroshio

Citation: Wang Lihua, Shi Benwei, Zhou Yunxuan, Sheng Hui, Gao Yanghua, Fan Li, Yang Ziheng. 2021. Radial velocity of ocean surface current estimated from SAR Doppler frequency measurements—a case study of Kuroshio in the East China Sea. Acta Oceanologica Sinica, 40(12): 135–147, doi: 10.1007/s13131-021-1883-2

1 Introduction

The ocean current is an important form of seawater movement. They affect the transport of material through the ocean and have a significant impact on the formation and evolution of climate and weather patterns over the ocean and across the globe (Klemas, 2012). Currents flowing towards high latitudes drive the upward transport of water vapor, causing air humidity to increase and precipitation to occur. In contrast, currents flowing towards low latitudes have the reverse effect on temperature, inhibiting the upward transport of water vapor. The weak evaporation associated with the latter currents means that precipitation does not readily occur (He et al., 2020). The study of ocean currents provides an in-depth understanding of the interactions between oceans, land, and atmosphere, and is necessary for early warning of marine hazards.

Direct ocean current measurements have high accuracy but limited spatial coverage due to their high cost. This makes it difficult to fully capture the temporal and spatial changes to ocean currents, which are required in many applications. Numerous remote sensing radar observations have shown surface signatures that are related to the dynamics of the upper ocean at meso- and submeso-spatial scales (Johannessen et al., 1996; Romeiser et al., 2010; Liu et al., 2019; Moiseev et al., 2020). Altimeter, high frequency radar, and synthetic aperture radar (SAR) measurements provide important observations of ocean currents. Altimeter measurements of sea surface flow have a wide spatial coverage but a low spatial resolution (about 25 km), which means that they cannot resolve small-scale dynamic ocean processes, and data within 50 km of the coast are typically invalid (Krug et al., 2010; Quilfen and Chapron, 2019). Measurements from high frequency

Foundation item: The National Natural Science Foundation of China under contract Nos 42176174 and 41706196; the Open Research Fund of the State Key Laboratory of Estuarine and Coastal Research under contract No. SKLECKF202104; the Zhejiang Provincial Natural Science Foundation of China under contract No. LY22D010002; the National Science Foundation for Post-doctoral Scientists of China under contract No. 2020M683258; the Chongqing Technology Innovation and Application Development Special Project under contract No. cstc2020jscx-msxmX0193; the Sichuan Science and Technology Program under contract No. 2018JY0484.
*Corresponding author, E-mail: wanglihua1@nbu.edu.cn

radar typically cover areas within 400 km of the shore and it is difficult to obtain data for open sea areas (Essen et al., 2000; Han et al., 2017). The Doppler frequency shift information of the SAR echo signal can reflect the dynamic characteristics of the sea surface, has become an essential sea surface dynamic remote sensing parameter. Therefore, SAR has unique advantages that make it an effective means of measuring sea surface flow. In addition, SAR observations have high spatial resolution and wide spatial coverage; measurements are available from multiple modes, and can be made in all weather conditions (Lehner et al., 2002).

Studies of sea surface flow based on SAR data can be grouped into two categories, one is the along-track interferometric SAR (ATI-SAR) technology, the other is the Doppler frequency technology. The ATI-SAR method was proposed by Goldstein et al. (1989) and has been validated for airborne (Graber et al., 1996; Romeiser, 2005) and spaceborne (Romeiser et al., 2010; Liu et al., 2019) SAR data. Acquisition of ATI-SAR data requires two along-orbit antennas, separated by a specific distance, to receive complex SAR images within a time difference of milliseconds. Detection of moving targets within the images then allows the current velocity to be monitored. However, on the one hand, acquisition of ATI-SAR data at present is subject to atmospheric interference that affects the timeliness and coherence of images (Rio et al., 2014; Yoshida and Rheem, 2015; Liu et al., 2019). On the other hand, the sea surface current results retrieved from ATI-SAR data still lack detailed result validation and analysis (He et al., 2020). Many satellites equipped with SAR sensors have been launched, and many researches are therefore focused on exploring new technology and inversion techniques for retrieval of sea surface flow from SAR measurements. SAR wave mode data have been used to find the global sea surface Doppler velocity in a study that also confirmed that the Doppler frequency shift is closely related to characteristics of the local environment (Chapron et al., 2004). A further study derived a relationship between the Doppler velocity and sea surface wind speed, and proved theoretically that the Doppler spectrum contains quantitative information about sea surface flow (Chapron et al., 2005). One study used the Doppler centroid anomaly method to derive the Agulhas flow from advanced SAR (ASAR) wide swath mode (WSM) images, and compared it with measured buoy and altimeter data (Krug et al., 2010). Sources of error in the inversion method used to derive ocean current from SAR data have been pointed out and a correction for these has been proposed in Hansen et al. (2011a). Subsequently, the inversion method has been used to derive ocean current velocities in the Changjiang River (Yangtze River) coastal zone (Wang et al., 2014b), in the Agulhas current zone (Johannessen et al., 2008; Krug et al., 2010) and in the Norwegian Sea area (Hansen et al., 2011b; Moiseev et al., 2020). Studies have verified the feasibility of using SAR data to detect temporal and spatial variations in surface current velocities. The SAR therefore has an increasingly considerable role to play in quantitative studies of ocean surface current features. Doppler frequency information has also gradually become an important remote sensing parameter of sea surface dynamics. The development of the SAR Doppler technology offers new possibilities to observe and model mesoscale and sub-mesoscale oceanic processes and sea surface current phenomena (Johannessen et al., 2008; Mouche et al., 2012; Wang et al., 2014b; Moiseev et al., 2020).

The Kuroshio is a fast-flowing, warm, and highly saline ocean current and is an important component of the North Pacific subtropical circulation system (Zhuang et al., 2020). The main flow of the Kuroshio in the East China Sea (ECS) follows the steep edge of the continental shelf (Fig. 1). A more detailed schematic representation of the flow in and around the Kuroshio in the ECS can be found in Qiu and Lukas (1996), Ma et al. (2009), and Zhuang et al. (2020). The Kuroshio is an important circulation system for China coastal seas. Seasonal and interannual variations in the Kuroshio also have a strong impact on regional cli-

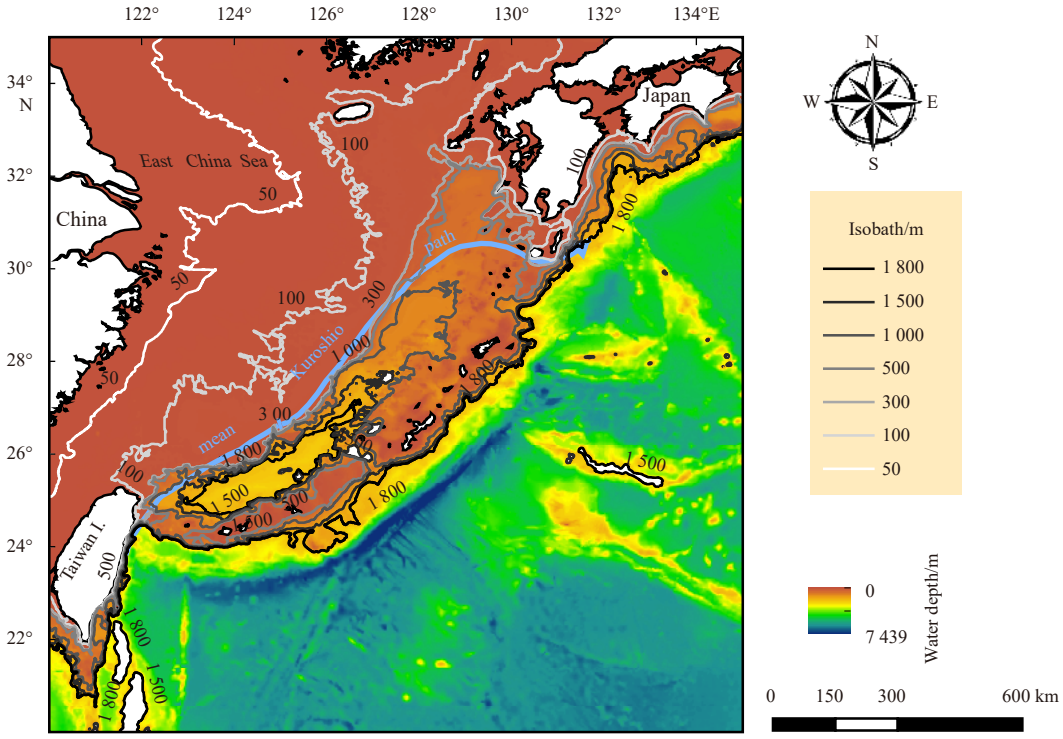

Fig. 1. Bathymetry of the East China Sea. The blue line is a schematic representation of the mean path of the Kuroshio, according to Ma et al. (2009), Qiu and Lukas (1996), and Zhuang et al. (2020).

mate.

Both the implementation of the International Strategic Plan about the Kuroshio and the publication of Science Citation Index Expanded (SCIE) research papers about the Kuroshio have been analyzed (Zhang et al., 2017). The analysis results show that research of the Kuroshio in the ECS has focused on the characteristics of the temporal and spatial changes of the Kuroshio path, the Kuroshio flow rate, the formation mechanism of the Kuroshio current and the heat transport associated with the Kuroshio current. In recent years, numerical analysis and simulation have been used to study the Kuroshio and model studies have resulted in much progress (Guo et al., 2006; Qiu et al., 2020); however, simulation results are strongly affected by fluxes at the open domain boundary. Steep submarine topography and strong baroclinicity in the Kuroshio make it difficult to calculate the seabed topography and pressure gradient force precisely (Jia et al., 2013; Qiu et al., 2020). Marine remote sensing technology has provided abundant high-resolution images and analysis methods that can be used to study the Kuroshio in the ECS. Integrating data from Argo floats with satellite altimeter data give a time-series of sea surface velocities for the Kuroshio and adjacent regions (Ma et al., 2009), and data for the Kuroshio central flow show that the mean current speed increases gradually from 0.65 m/s south of Kyushu to 1.45 m/s off Enshu-nada (Ambe et al., 2004; Deng et al., 2015). Altimetry provides an indirect (geostrophic-based) measurement of the sea surface flow. However, at the Kuroshio region in the ECS, the main body of the Kuroshio current is relatively stable and follows closely along the steep continental slope due to the topographic constraint (Zhuang et al., 2020), which makes it very difficult for altimeters to accurately capture the mean flow dynamic from sea level anomaly measurements (Krug et al., 2010). While SAR measurements have the capability to provide a direct observation of the Kuroshio surface current in the radar range direction on spatial scales from 2 km to 10 km, which is better than the ocean currents measured by altimeter on a spatial resolution of 25 km (Wang et al., 2014b). Satellite ENVISAT advanced synthetic aperture radar (ASAR) data cover a long time period, and include multi-mode images with reliable quality, which are helpful for studying the structure and transport characteristics of ocean currents. The capability of ENVISAT ASAR data studying the ocean current velocities has been demonstrated (Chapron et al., 2005; Johannessen et al., 2008; Wang et al., 2014b). However, the inversion of ocean currents based on the Doppler center shift method requires specific analysis of ocean phenomena of different scales at different spatial resolutions. The error of ocean current observations largely depends on the temporal and spatial scales of the ocean currents measurement. At present, the verification of the SAR ocean current inversion results is still insufficient. The cross-validation of different ocean current products from remote sensing data and the analysis of the inversion results still lack comprehensive discussion and research (He et al., 2020). Therefore, we begin by calculating the radar Doppler center frequency, then separate out the components of Doppler frequency caused by non-ocean currents, and construct Doppler centroid frequency anomaly algorithm of ocean current to derive the radial Doppler surface current of the Kuroshio in the ECS based on the ENVISAT ASAR data. Following this, we finally carry out a detailed accuracy assessment and sensitivity analysis for the radial velocity derived from the SAR imagery. This work will promote and contribute to improvements in the monitoring of ocean currents using SAR data, and will result in a complete time-series of ocean current data useful to studies of the variability and impacts of the Kuroshio. Data from this work will also provide useful boundary constraints for future analyses of the mechanisms that drive the formation and development of the Kuroshio.

The structure of this paper is as follows: in Section 2, the SAR imagery and the data used for validation, accuracy assessment, and sensitivity analysis are introduced; and the algorithm for calculating anomalies in the Doppler frequency is described; in Section 3 the Doppler centroid frequency and radial Doppler velocity calculated for the Kuroshio are presented; in Section 4, we present an accuracy assessment and sensitivity analysis for the current SAR measurements; and in Section 5, we present our conclusions.

2 Data and methods

2.1 *Data*

2.1.1 *SAR data*

We use ASAR WSM mode C-band (5.3 GHz) images, acquired at an incidence angle between 16° and 43°, with a wide spatial coverage of approximately 420 km^2. A total of 2 ascending and 6 descending ASAR WSM images, acquired over the Kuroshio in the ECS, were obtained from the European Space Agency and are used to derive the surface radial Doppler velocity (Table 1 and Fig. 2).

Doppler centroid estimation is a key element to our SAR data processing. The grid of Doppler centroid frequencies has dimensions corresponding to the sensor range and azimuth direction (Table 1). The change in frequency with range direction depends on the satellite attitude and on how closely the ground footprint is related to the range; there are usually 100 grid cells in the range direction. The change in azimuth direction accounts for the relatively slow change in satellite attitude as a function of time. The normalized radarcross section (NRCS) of the ASAR WSM ascending scene over Kuroshio in the ECS on 26 July 2007 and descending scene on 28 May 2008 are presented in Fig. 3.

2.1.2 *Ocean current validation data*

Global ocean multi-observation (MOB) products (http://marine.copernicus.eu), MULTIOBS_GLO_PHY_REP_015_004, with

Table 1. ENVISAT advanced synthetic aperture radar (ASAR) wide swath mode (WSM) products description

Acquisition time (UTC)	Polarization	Doppler centroid numbers (range by azimuth)	Orbit	Track	Pass
2007-07-26 13:29:03	VV	100×115	28249	139	ascending
2007-11-13 01:22:38	VV	100×70	29816	203	descending
2007-11-29 01:19:42	VV	100×70	30045	432	descending
2007-12-02 01:25:27	VV	100×70	30088	475	descending
2007-12-18 01:22:36	VV	100×70	30317	203	descending
2008-01-31 01:39:52	VV	100×70	30947	332	descending
2008-05-28 01:31:19	HH	100×54	32636	017	descending
2011-08-02 13:19:29	VV	100×67	49277	125	ascending

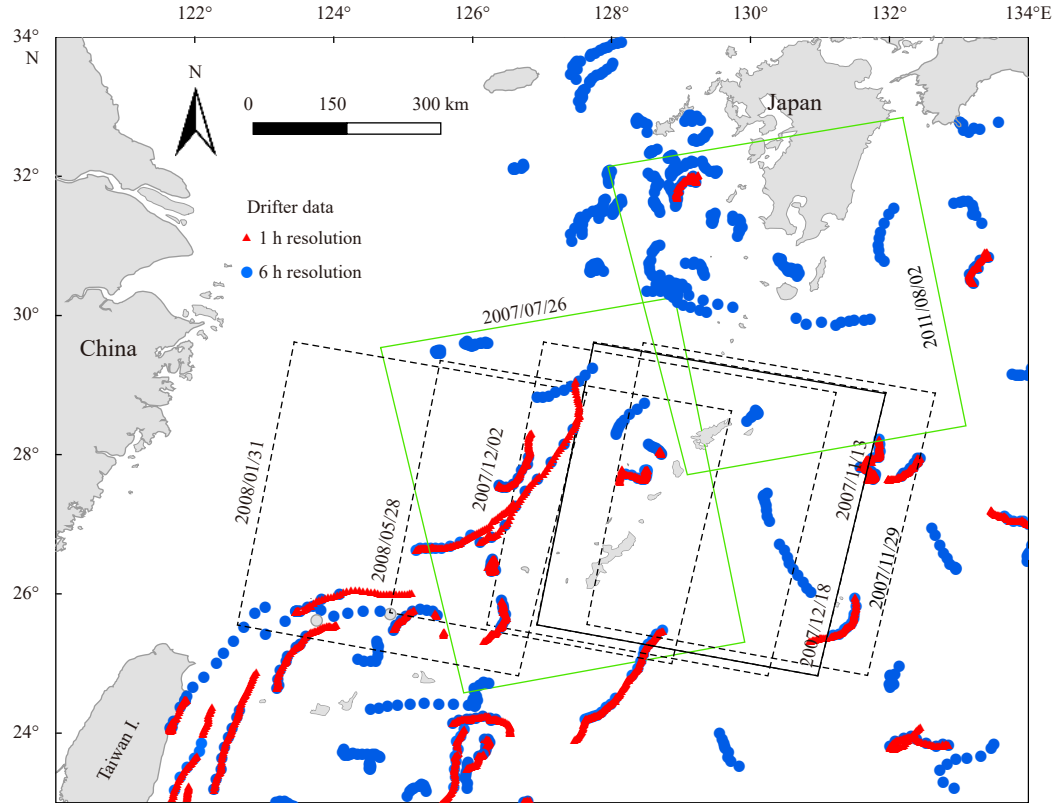

Fig. 2. Location of advanced synthetic aperture radar (ASAR) images and surface drifter data. The rectangles show the areas covered by the ASAR images: green and black denote images from ascending and descending orbits, respectively. The dots represent drifter data: red and blue denote data 1-h and 6-h resolutions, respectively.

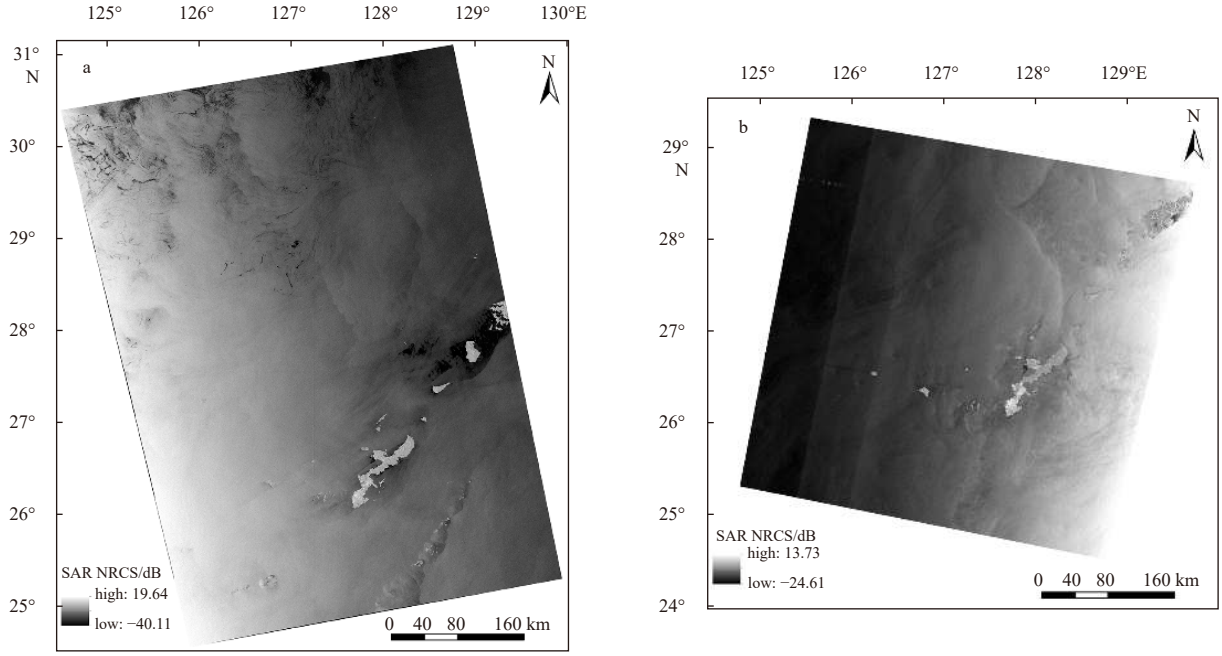

Fig. 3. The synthetic aperture radar (SAR) normalized radarcross section (NRCS) image on July 26, 2007 (a), and May 28, 2008 (b).

(1/4)° horizontal resolution and two vertical levels (surface and 15 m), are the sum of the geostrophic and Ekman components of the surface and near-surface current. Data from Argo floats from 2001 to 2007 are used to estimate the accuracy of the surface products. The root mean square error (RMSE) values for the zonal and meridional surface velocity products are 0.146 m/s and 0.147 m/s, respectively, and the correlations between these products and the Argo float data have R^2 values of 0.82 and 0.73, respectively. One of the MULTIOBS_GLO_PHY_REP_015_004 products, "Dataset-uv-rep-hourly", includes the three hourly

zonal and meridional velocity fields and has been shown to be highly accurate (Rio et al., 2014). MOB products have wide spatial coverage, are readily accessibility, and have high data quality, and have therefore been important for verifying the accuracy of satellite-derived estimates of surface current velocity (Chapron et al., 2005; Krug et al., 2010).

Global surface Lagrangian drifter (GLD) data are ocean current velocities calculated from position information recorded by drifting buoys. They are stored at the Drifter Data Assembly Center at NOAA'S Atlantic Oceanographic and Meteorological Laboratory (https://www.aoml.noaa.gov/envids/). Data are processed, quality controlled, and optimally interpolated (via kriging) to uniform 6-hourly intervals and then made publicly available. Hourly drifter data were released on 18 July 2019 (Version 1.03) and are a subset of the 6-hourly data. To select buoy data to compare to a SAR velocity for validation, buoy data were required to be recorded within 12 h and 24 h of the SAR acquisition time, and to be within a 5-km radius of the SAR image location. Velocity from the closest of these selected buoy data points was used for comparison with the SAR velocity. A total of 17 collocations within 12 h and 162 collocations within 24 h in the study were identified to validate the SAR velocities (Fig. 2).

2.2 *Methods*

We use the Doppler frequency shift theory in our inversion method for deriving the surface current from SAR imagery. This involves first removing contributions from the Doppler centroid frequency f_{Dc} that are attributable to factors other than ocean surface currents. Values for f_{Dc} are calculated from the echo signal at the satellite using the Doppler centroid method and so include the Doppler frequency f_{Dp} caused by the relative motion of the satellite and the Earth, which must be removed. The Doppler centroid frequency of the sea surface echo also includes the Doppler frequency shift attributable to sea surface motion other than surface currents, such as gravity wave motion, orbital wave motion, Stoke's drift, and nonlinear hydrodynamic effects between waves; these contributions also need to be removed. After removing the above effects, the remaining Doppler frequency shift f_g is attributable to the overall movement of the seawater and the radial velocity of the surface current can be calculated. Figure 4 shows the above steps in a flow chart.

2.2.1 *Original Doppler frequency anomaly (f_{Dca})*

A grid of Doppler centroid frequency values f_{Dc} is provided for ASAR WSM data with the ASAR WSM level-1b products. Four functions from the ENVISAT CFI software libraries (*pl_emjd*, *pp_init_attitude_file*, *pp_get_attitude_aocs*, and *pp_target*) are called to calculate f_{Dp} and to obtain the geographical footprint location (Wang et al., 2014a). Original Doppler frequency anomaly, f_{Dca}, is defined as f_{Dc} minus f_{Dp}, and is attributable to the combined action of near surface wind on shorter waves, longer wave motion, wave breaking, and surface currents. To identify the part of the anomaly attributable to ocean currents, f_{Dca} must be separated into components attributable to different contributing sources.

2.2.2 *Geophysical Doppler frequency anomaly (f_g)*

The estimation errors f_{err}, such as the azimuthal variation of NRCS, antenna mispointing and strong discrete targets, that contaminate the geophysical Doppler shift information, must be eliminated first. This error correction is carried out by finding the linear relationship between the azimuthal gradients of backscatter variation in a single Doppler frequency grid and gradients of Doppler centroid anomaly along azimuth over land cover (Chapron et al., 2005; Johannessen et al., 2008; Hansen et al., 2011a; Mouche et al., 2012; Wang et al., 2014b).

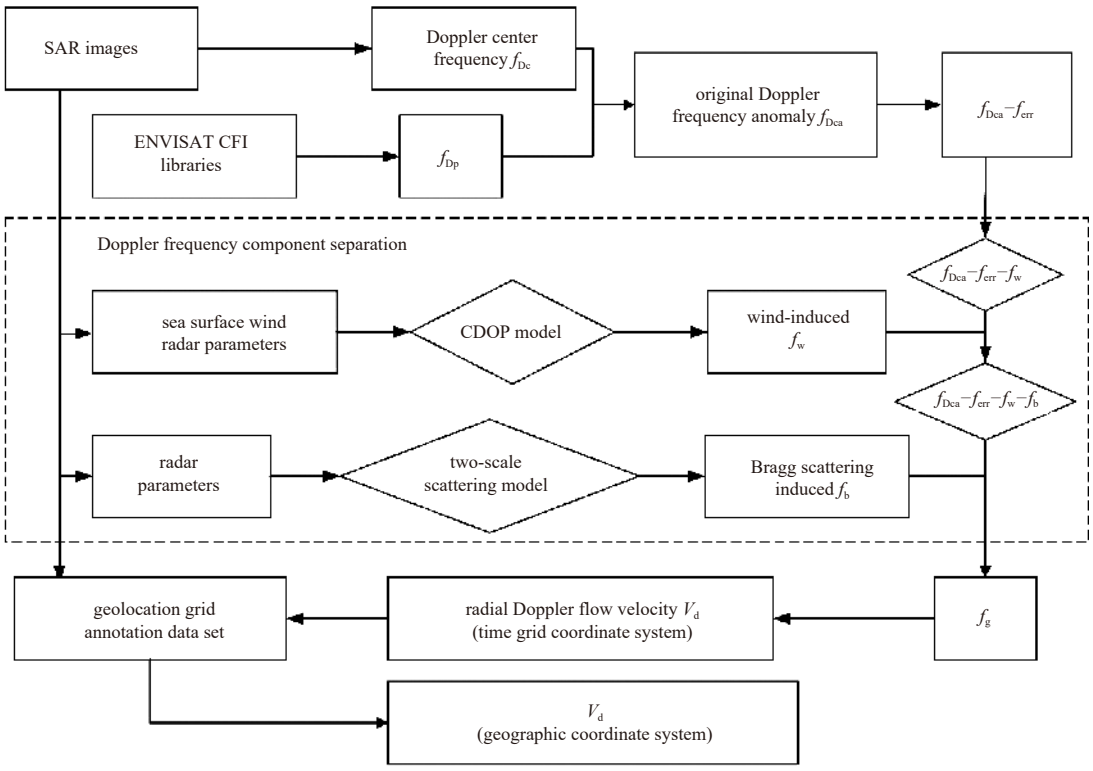

Fig. 4. Flow chart of the inversion method for calculating ocean current from synthetic aperture radar (SAR) data based on Doppler frequency theory.

The sea surface wind contribution to the Doppler frequency comes mainly from wave orbital motion, but first order effects also include Ekman drift and Stoke's drift (Johannessen et al., 2008; Hansen et al., 2011a). Accurate estimation of the sea surface wind vector is essential for calculation of the wind-induced Doppler frequency, f_w. The wind vector that is derived from inversion of the SAR image has high precision and matches perfectly in space and time with the ocean current monitoring data, since it is derived from the same SAR image (Lin et al., 2008). Wind direction is derived from SAR images using 2D fast Fourier transforms and the 180° directional ambiguity are removed according to the blended sea winds dataset (Wang et al., 2014a). These blended winds are obtained from blending observations of multiple satellites at the National Center for Environmental Prediction (NCEP) and reanalysis 2 products from the European Centre for Medium-range Weather Forecasts (ECMWF) (https://www.ncdc.noaa.gov/data-access/marineocean-data/blended-global/blended-sea-winds). Wind speed is retrieved using a C-band model (Wang et al., 2014a). An empirical geophysical model function (CDOP) was employed to calculate the wind-induced Doppler shifts contribution f_w to the SAR Doppler center frequency. And the f_w depends on the wind speed, radar incidence angle, polarization, and wind direction with respect to radar look direction (Mouche et al., 2012), and then remove it from f_{Dca}.

Following the two-scale microwave scattering model, simulated ocean waves include large-scale fundamental waves and small-scale gravity waves, which, for incident radar waves, generate specular reflection and Bragg scattering, respectively. The radar sea surface echo is mainly modulated by Bragg scattering, and the spatial resolution of ENVISAT ASAR WSM data is too coarse to identify large-scale waves, so the contribution to the Doppler shift from Bragg scattering f_b, can be obtained from the relationship between gravity waves and dispersion (Toporkov and Brown, 2000; Li et al., 2020), $f_b = \pm\frac{1}{2\pi}\sqrt{2g_0 k\sin\theta}$, where g_0 is the acceleration of gravity (m/s^2); k denotes the radar incident wave number (m^{-1}), and θ is the incident angle. And then, the geophysical contribution to the Doppler frequency anomaly, f_g, can then be found from the following equation:

$$f_g = f_{Dca} - f_{err} - f_w - f_b. \tag{1}$$

2.2.3 *Radial doppler velocity (V_d)*

The radial Doppler velocity calculated from the geophysical Doppler frequency anomaly is assumed to be a measurement of the radial surface velocity, according to:

$$V_d = -\frac{\pi f_g}{k_e} = -\frac{\overline{\upsilon_r \delta_0}}{\bar{\delta}_0}, \tag{2}$$

where k_e is the electromagnetic wavenumber, which is 112 m^{-1} for the ENVISAT ASAR instrument, and f_g is related to the spatial mean of the range component of the sea surface scattering elements, υ_r, weighted by the local normalized radar cross section (NRCS) δ_0.

3 Results

3.1 *Doppler centroid frequency*

The Doppler centroid frequencies, f_{Dc}, determined from an ascending SAR scene on July 26, 2007, and from a descending scene on May 28, 2008, are presented in Fig. 5. Modem-phased antenna arrays are subject to variations in azimuth angle throughout the subswath and jumps in the Doppler centroid frequency are clear at subswath boundaries in Fig. 5 due to this active antenna behavior.

Taking the Doppler frequency anomaly for the SAR image on July 26, 2007 as an example, the root mean square (RMS) for f_{Dca} is 17.70 Hz after f_{Dp} has been removed. After removal of f_w, f_b and f_{err}, the RMS for the Doppler frequency anomaly for this image reduces to 16.42 Hz and 14.32 Hz, respectively. As for the Doppler

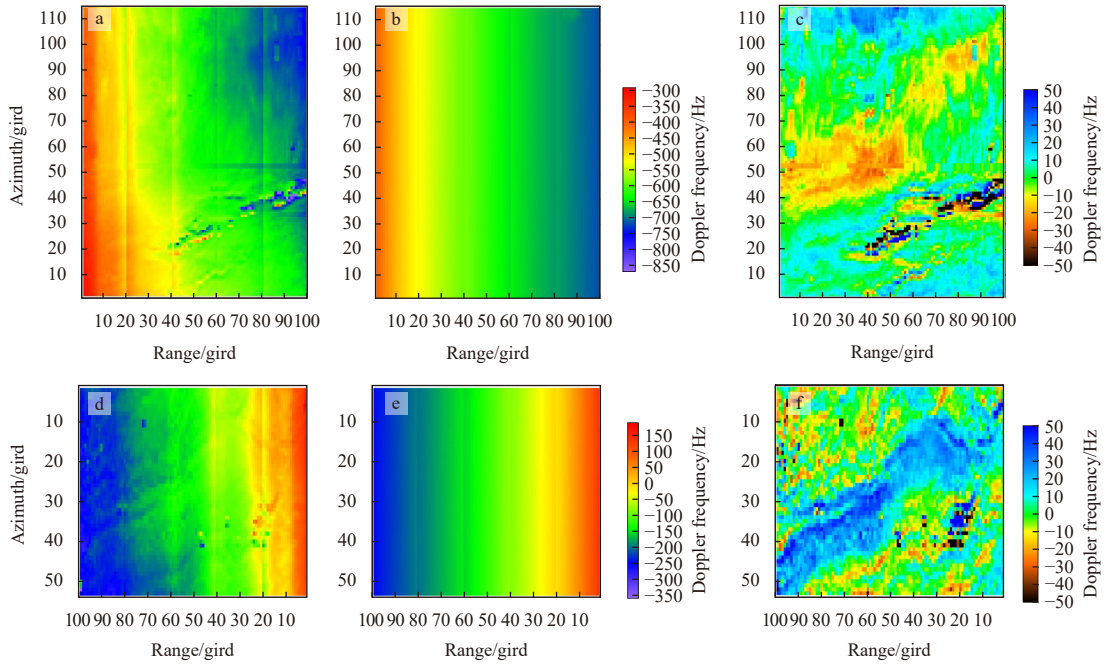

Fig. 5. The Doppler centroid grid f_{Dc} (a), f_{Dp} (b) and f_{Dca} (c) from ascending SAR scene on July 26, 2007; and f_{Dc} (d), f_{Dp} (e) and f_{Dca} (f) from SAR descending scene on May 28, 2008.

frequency shift over land, the mean Doppler anomaly is reduced from 20.1 Hz of the raw Doppler anomaly to 9.7 Hz after the error correction. Because of the strong azimuthal NRCS gradients, there are still absolute values of Doppler frequency anomaly greater than 30 Hz over land, even after the error correction. The mean value is further reduced to 6.3 Hz after invalidating these absolute values larger than 30 Hz. The other images are processed in the same way and the RMS values calculated for the Doppler frequency anomalies are shown in Table 2.

There is a large spread in the values calculated for f_g over Okinawa island, where the Doppler frequency is expected to be zero (Fig. 6). Much of the variability in f_g here is due to NRCS gradient in the azimuth direction, which is within the estimation area for the Doppler centroid grids.

3.2 *SAR radial velocity*

Figure 7a shows V_d in the ECS derived from the ascending, right-viewing SAR scene on July 26, 2007. Areas of the Kuroshio where $V_d > 0$ correspond to yellow, red, and black in Fig. 7a, showing that surface velocities are directed away from the satellite projection line, that is the central flow of the Kuroshio is meandering to the east/northeast along the Okinawa Trough. The velocity range is between 0.5 m/s and 1.0 m/s. V_d is interpreted to be the radial component of the true surface current, and thus Fig. 7a shows that the Kuroshio is not a single jet with broad uniform flow in the upstream direction. The current meanders with westerly and southwesterly flow reversals ($V_d < 0$, blue and purple in Fig. 7a) at (26.8°N, 127.2°E), at (27.4°N, 127.6°E), and at (27.8°N, 127.8°E). This is the Kuroshio Counter Current (KCC), which has a velocity range of 0.2 m/s to 0.6 m/s.

Figure 7b shows V_d derived from the descending, right-viewing SAR scene on May 28, 2008. Since these are derived from a descending SAR image, areas of the Kuroshio with $V_d < 0$ are yellow, red, and black in Fig. 7b, corresponding to a surface current directed towards the satellite flight projection line, that is the main flow of the Kuroshio is meandering to the east/northeast along the Okinawa Trough. The direction of the central flow of the Kuroshio that is derived from this image is consistent with that derived from the July 26, 2007 image, and the most of the velocities derived from this image are between 0.4 m/s and 1.2 m/s. Similarly, the current meanders found for the ascending image can also be seen here at approximately (27.0°N, 127.8°E), (26.6°N, 127.4°E), (26.2°N, 126.8°E), and (26.2°N, 127.4°E), where green and blue in Fig. 7b show $V_d > 0$, corresponding to a westerly or southwesterly flow in the descending image. The derived velocities for this counter flow in the image range from 0.3 m/s to 0.5 m/s. The results of the inversion for the descending SAR scene on May 28, 2008 clearly show the KCC and are consistent with the results for the July 26, 2007 scene.

4 Discussion

4.1 *SAR radial velocity comparisons with MOB and GLD*

To validate the sea surface flow characteristic obtained using SAR Doppler theory, we projected the MOB products and GLD data onto the SAR radial current direction.

Table 2. The RMS variation of Doppler frequency

Acquisition date for SAR scene	f_{Dc}	RMS for the Doppler frequency anomaly/Hz		
		f_{Dca}	f_{Dca}-f_w-f_{err}	f_g
Jul. 26, 2007	97.56	17.70	16.42	14.32
Nov. 13, 2007	109.55	15.80	14.80	13.65
Nov. 29, 2007	104.56	10.72	10.12	9.26
Dec. 2, 2007	110.13	15.53	14.49	13.41
Dec. 18, 2007	113.64	16.27	14.97	13.03
Jan. 31, 2008	112.58	9.22	8.51	5.91
May 28, 2008	101.89	12.25	11.80	10.82
Aug. 2, 2011	89.44	18.42	16.48	14.22

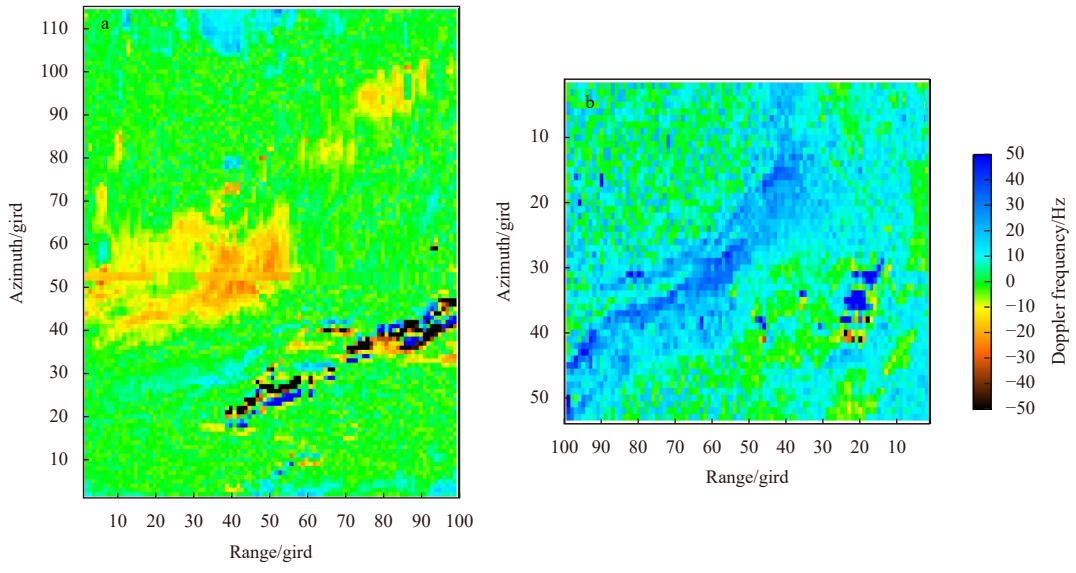

Fig. 6. The geophysical Doppler frequency anomaly f_g on July 26, 2007 (a), and on May 28, 2008 (b).

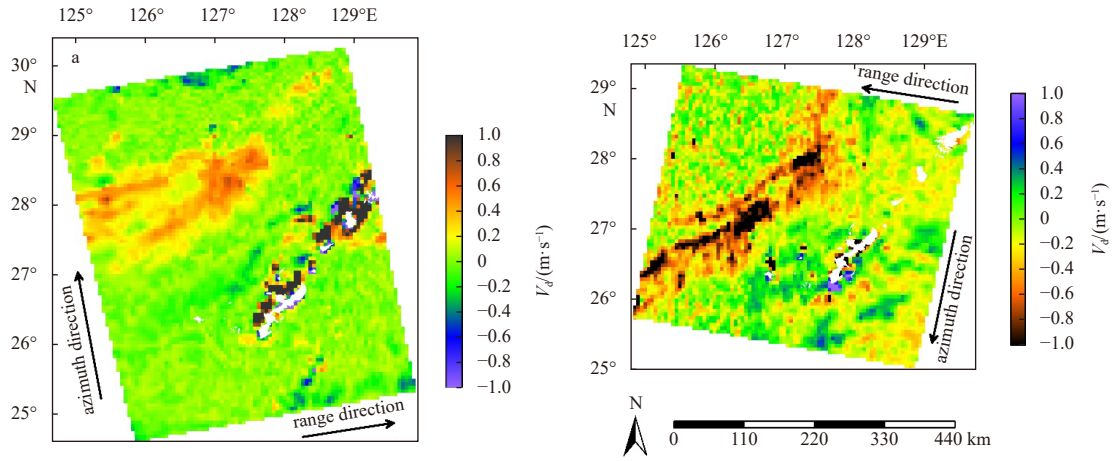

Fig. 7. The radial Doppler velocities derived from ASAR scenes on July 26, 2007 (a), and on May 28, 2008 (b). Land is shown in white.

The SAR surface radial currents found for July 26, 2007 and for May 28, 2008 were compared with the MOB products (Figs 8a and b). Both the SAR currents and the MOB products capture the direction and intensity of surface currents in the Kuroshio region and the two data sets are in good agreement (Figs 8a and b). In the center of the Kuroshio and in the KCC regions, the SAR flow direction is consistent with the MOB products, and is towards the northeast. The central flow velocity of the Kuroshio is high and the radial characteristics are clear. As a branch of the Kuroshio central flow, the KCC begins to turn around at (27.6°N, 127.8°E) and gradually turns to the southwest in the SAR-derived data, which coincides with the southwest counter current seen in the MOB products.

To illustrate in more detail how SAR scenes can be used to monitor ocean currents, transects from the central flow of the Kuroshio (the solid blue line in Figs 8a and b) and from the center of the KCC (the solid orange line in Figs 8a and b) are selected and compared with MOB data in Figs 8c and d. The spatial resolution of the SAR radial velocity is 8 km in the azimuth direction and varies from around 9 km for the near-range to around 3.5 km for the far-range in the range direction. The spatial resolution of the MOB products is 0.25° (approximately 25 km), which is significantly coarser than the SAR data (Figs 8c and d). There are clear differences between the intensity of the flow derived from the SAR data and in the MOB products. On July 26, 2007, the central flow velocity for the Kuroshio derived from the SAR data has a wide range of values, from 0.4 m/s to 1.5 m/s, while the MOB products report a narrower range of 0.5 m/s to 0.6 m/s (Fig. 8c).

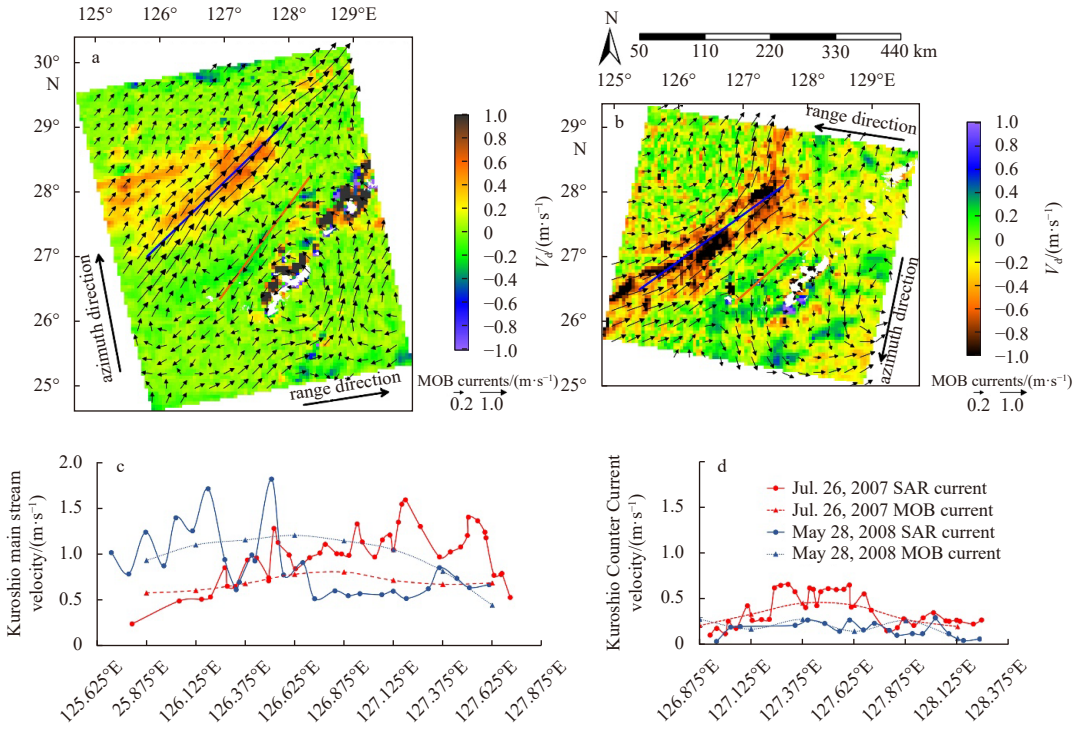

Fig. 8. The radial Doppler velocities from the SAR scenes on July 26, 2007 (a), and on May 28, 2008 (b) with the corresponding multi observation (MOB) products superimposed as arrows (arrow length indicates strength); and transects of SAR range velocity and MOB velocity on July 26, 2007 and May 28, 2008 for the Kuroshio central flow (c), and for the Kuroshio Counter Current (d).

The range of velocities derived for the KCC from the SAR data is 0.2 m/s to 0.6 m/s, while the MOB velocities range from 0.2 m/s to 0.5 m/s (Fig. 8d). On May 28, 2008, the central flow velocity for the Kuroshio from the SAR data is generally between 0.5 m/s and 1.5 m/s, while the MOB velocity range is more concentrated, and is generally between 0.5 m/s and 0.6 m/s, similar to the results for July 26, 2007 (Fig. 8c). Between around (27.2°N, 127.8°E) and (26.2°N, 126.4°E), the central flow of the Kuroshio begins to branch and gradually turns to the southwest, forming the KCC. Velocities derived from the SAR data, and reported in the MOB products are concentrated between 0.2 m/s and 0.3 m/s (Fig. 8d).

According to the MOB products on July 26, 2007 (Fig. 8a), the surface currents flow towards the northeast at speed of 0.4–0.5 m/s at approximately (26°N, 129°E). However, the SAR-retrieved velocities are low, 0.05–0.20 m/s, which are related to the corresponding low radar backscatter intensity (Fig. 3a). The inconsistencies in the measurements are probably that MOB product has coarse resolution, while high resolution SAR has advantages of resolving smaller scale current variations. Also, the SAR Doppler frequency is modulated by the effects related to wind-wave-current interactions (Johannessen et al., 2008; Krug et al., 2010; Mouche et al., 2012; He et al., 2020). In addition, the interaction between underwater topography and current, could affects the convergence and divergence of the sea surface current, in turn, takes an effect on the sea surface current retrieval from SAR. The main reason for these large inconsistencies is probably that the ocean current velocity detected by SAR is the ocean current radial velocity, it is not sensitive to the azimuth velocity. The ocean current velocity at this location is more concentrated in the azimuth direction, which is not conducive to SAR detection. Therefore, the value of SAR detection is low. The SAR scene on May 28, 2008 is a descending orbit image. Thus, the SAR sensor is on the right side of the image. According to the MOB products, the current direction is northwest/west at (28°N, 129°E), so the SAR current should be positive. Yet, the retrieved SAR current shows negative V_d in green to yellow (Fig. 8b). The velocities of ocean current flow at this location fluctuate between 0.2 and –0.2, the value is small. Therefore, the error of the Doppler frequency shift may cause a change in the sign of the SAR ocean current, in turn, an inconsistency occurs between SAR result and MOB product. In addition, this area is exactly at the position where the direction of the ocean current changes, the Doppler frequency and the SAR radial current are subject to many factors such as satellite motion, wind and waves, which result in the uncertainty of SAR ocean current (He et al., 2020).

The statistical error associated with the radial current derived from eight SAR scenes was found through comparison with the MOB products and is shown in Fig. 9a. The number of matched samples is 1 888. The error distribution is an approximate standard normal distribution, with the 90% confidence interval concentrated between –0.1 m/s and 0.1 m/s. The standard deviation is 0.275 m/s. A few outliers negatively impact the overall performance of the retrieval method for surface current velocities from SAR data. The number of matched samples that correspond to an absolute error exceeding 0.5 m/s is 142, which is 7.5% of the total number of matched samples. Careful manual inspection shows that these outliers are mainly located on Okinawa Island, or in a 10 km buffer zone around it, and could therefore be attributed to high radar backscatter variability within the azimuth beam width of the SAR antenna. The statistical errors found by comparing the radial current velocities derived from the 8 ASAR scenes with the GLD range velocities are shown in Figs 9b and c. From 162 collocated data points within 24 h of the SAR acquisition time, concentrated in the Kuroshio region in the ECS, the RMSE is 0.186 m/s. When the ocean current velocity is in the range of 0.4—0.7 m/s, the SAR retrievals are smaller than the GLD products. There are two possible reasons for the underestimation of SAR ocean current. First, the influence of sea surface wind, Bragg scattering, the offset of the backscattering coefficient in a single Doppler pixel and other factors were fully considered. The correction of these factors may cause over-correction of Doppler frequency shift, which is probably a main reason (He et al., 2020). Second, in the process of SAR remote sensing ocean current monitoring, the calculation of Doppler frequency is affected by many factors such as satellite motion, complex sea surface scatter, and complex wind-wave interaction. All these factors need to be considered, which could cause errors in the calculation (Chapron et al., 2005; Johannessen et al., 2008; Wang et al., 2014b; Moiseev et al., 2020). As demonstrated in Fig. 9c, the result of the comparison between SAR ocean current velocities and GLD products has improved, with the RMSE reduced from 0.186 m/s to 0.148 m/s, after shorting the time window to 12 h. However, it is undeniable that the available collocated data points have also been greatly reduced from 162 to 17. From the overall comparative analysis, the correlation between the SAR-derived and GLD data, the r^2 value is 0.803 at the time window of 24 h, when the time is limited to 12 h, the r^2 value is 0.889. The t-test shows both of the correlation coefficients are significant at a confidence level of 99%. We therefore state that ocean current velocities retrieved from SAR imagery have a high accuracy and have the potential to fully

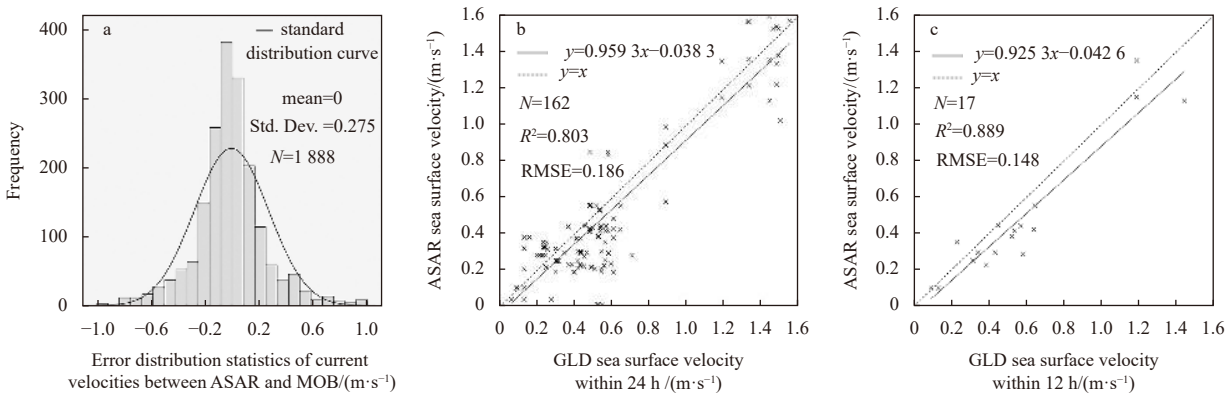

Fig. 9. Error analysis of the radial velocities. a. Comparing SAR-derived data with the multi observation (MOB) products. b and c. Comparing SAR-derived data with the global surface Lagrangian drifter (GLD) data with the time window of 24 h (b) and 12 h (c).

capture the current flow dynamics (Chapron et al., 2005; Krug et al., 2010; Hansen et al., 2011b).

4.2 *Kuroshio characteristics in the ECS*

The Kuroshio is a large-scale, stable seawater flow. The image mosaic for the SAR-derived current reveals the characteristics and structure of the Kuroshio (Fig. 10). $V_d > 0$ m/s from the ascending, right-viewing SAR scene (on 26 July 2007 and 2 August 2011) corresponds to the surface velocities away from the satellite sensor, whereas $V_d < 0$ m/s from the descending, right-viewing SAR scene (28 May 2008) indicates a flow towards the sensor. That is the main flow of the Kuroshio is meandering to the east/northeast along the Okinawa Trough. The velocity for the Kuroshio derived from the SAR is 0.1–1.5 m/s, which shows that the SAR has the capability to monitor current velocity over a wide range of values.

Figure 10 clearly shows that the path of the Kuroshio closely follows the steep edge of the continental shelf. The left side of the Kuroshio flow meets the outer edge of the continental shelf, where the water depth is 100–300 m, and the right side of the flow meets an area of sloping seabed uplift (Qiu and Lukas, 1996; Jia et al., 2013; Zhuang et al., 2020). The axis of the Kuroshio central flow is adjacent to both the continental shelf and the slope, where water depth increases sharply and the seabed terrain is steep. At around (28°N, 126.5°E), where the water depth changes from 300 m to 500 m, and from 500 m to 1 000 m, the horizontal distance across the Kuroshio is just 2 km and 5 km, respectively (Fig. 10). This demonstrates that the changes in the flow of the Kuroshio are strongly constrained by underwater terrain (Guan, 1979; Deng et al., 2015). Around 30°N and 128°–129°E, the Kuroshio current detaches from the continental slope and veers to the east.

4.3 *Sensitivity analysis for SAR radial velocity*

The SAR data are processed on the basis that the Doppler centroid frequency provides the best possible signal-to-noise ratio and has high azimuthal resolution. In terms of radar echo signal reception, the Doppler centroid dataset f_{Dc} released with the ASAR WSM product includes the baseband Doppler centroid frequency, not the absolute Doppler frequency, which would be higher (European Space Agency, 2007).

The value of f_{Dp}, generated by the relative motions of the satellite and the Earth, is key to the inversion method used to derive surface current velocities from SAR. Electronic mispointing, inaccurate satellite orbit and attitude parameters (yaw, pitch, and roll), areas of low signal-to-noise ratios, and scenes that include some particular targets (for example, strong backscattering objects), can all introduce a bias to the values calculated for f_{Dp}, and any bias would be carried into the calculations for f_{Dca} and f_g.

The complex motion of sea surface waves is another potential source of error that may affect the accuracy of retrieved surface current velocities. If we assume the dual-scale microwave scattering model, then the sea surface is composed of small-scale irregular waves superimposed on large-scale waves. The echo scattered from the sea surface is mostly accounted for by Bragg scattering from small-scale waves, modulated by large-scale waves (He, 2000). The effect of Bragg scattering on the Doppler frequency varies with the SAR incidence angle, and for ENVISAT ASAR images this results in a contribution to the Doppler frequency of between 3.9 Hz and 6.2 Hz. In addition to Bragg scattering, there are tilt-, hydro- and aero-dynamic effects that modulate the scattered signal and these can also generate shifts in the Doppler frequency.

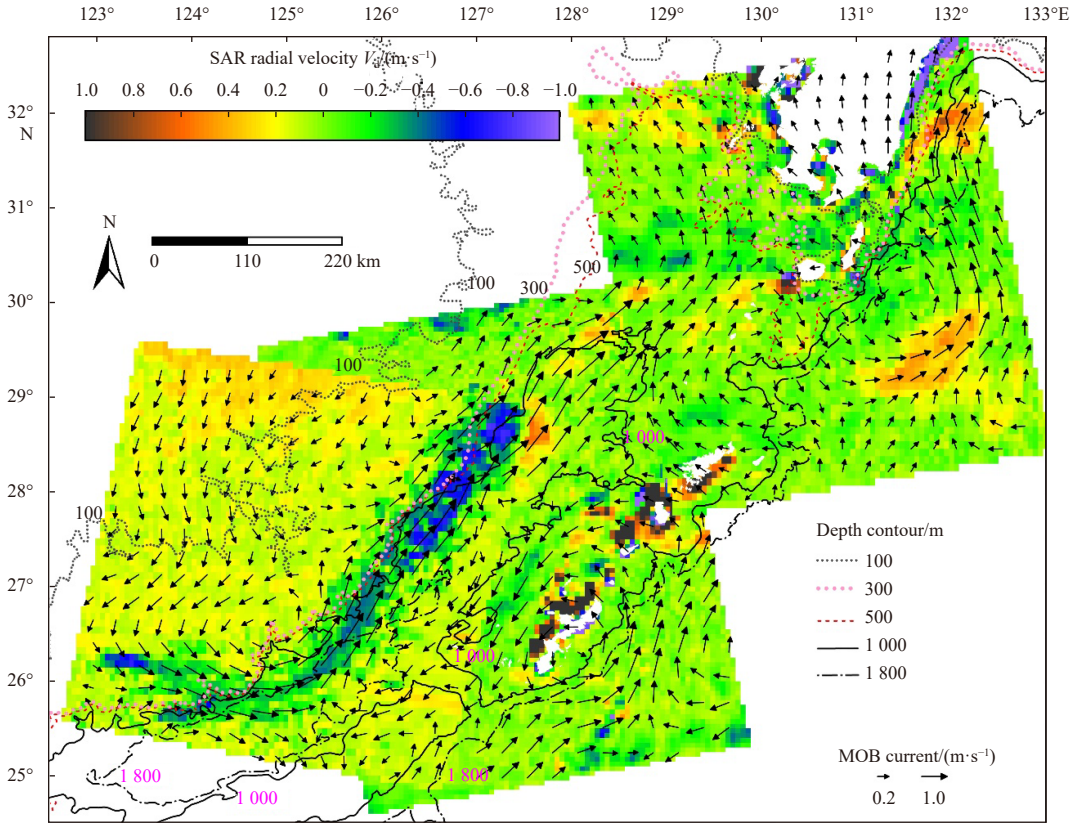

Fig. 10. Composite of SAR radial velocities derived from an ascending scene acquired on 26 July 2007 (middle), an ascending scene acquired on 2 August 2011 (upper right), and a descending scene acquired on 28 May 2008 (lower left).

When a strong Doppler signal passes through the radar antenna lobe, the NRCS gradient across the imaged scene means that the signal from the brightest part of the scene will contribute disproportionately to f_{Dc} (Chapron et al., 2005; Wang et al., 2014a). This effect is more pronounced when the NRCS varies significantly within the width of the SAR azimuth beam as occurs, for example, when SAR images are acquired over land-water boundaries as seen in Fig. 5. Values for f_{Dc} may therefore be distorted by the relatively stronger or weaker intensity of the signal away from the center of the radar beam. In this study, there is a strong NRCS gradient around the sea-land interface along the edges of the Okinawa Trough and values for f_g are very high in that area, generally between ± 70 Hz and ± 80 Hz (Fig. 6). These values correspond to radial Doppler velocities ranging from 1.96–2.24 m/s, and so values retrieved for V_d in that area are highly uncertain.

The radial Doppler velocity is the latitudinal component of the real current vector, relative to the azimuth direction for the SAR image. The surface current derived from SAR data therefore corresponds to the real current velocity, but is smaller, and this difference depends strongly on the radar incidence angle. At low incidence angles, returned radar echoes are stronger and more sensitive to larger and faster roughness elements (Krug et al., 2010), which leads to an increased contribution to the measured velocity from vertical components. The strong relationship between wind intensity and short-period waves means that, as the incidence angle decreases, the relative influence of wind on the Doppler anomaly increases (Krug et al., 2010). Previous studies have found a sudden increase in the Doppler velocity error for SAR data when the radar incidence angle decreased below 30°. At radar incidence angles greater than 30°, the radial current velocity retrieved from SAR data approximates the true current more closely (Wang et al., 2014a). The radial Doppler current derived from SAR data reflects the trends and intensity of the current movement, but it cannot fully capture the flow direction. This is a consequence of the single directivity of the Doppler frequency shift.

Numerical simulation experiments show that obtaining high-precision surface current velocity from SAR images requires an accurate sea surface wind to be input (Mouche et al., 2012). A blended sea surface wind field, derived from a combination of U.S. National Center for Environmental Prediction (NCEP) and European Centre for Medium-range Weather Forecasts (ECMWF) products, is compared with the wind field retrieved from the SAR data using a 2D fast Fourier Transform and the CMOD4 model. The comparisons show that the RMS for the SAR-derived wind direction is 8°, and for wind speed the RMS is 1.0 m/s. The maximum error in SAR radial velocity that could be driven by these errors is about 0.1 m/s (Wang et al., 2014b). If inaccurate sea surface wind direction is input to the CDOP model, it leads to large errors in the retrieved SAR range velocity and significantly reduces the inversion accuracy (Chapron et al., 2005; Krug et al., 2010; Wang et al., 2014a). Retrieval of the sea surface wind field from the SAR image itself is therefore helpful for improving the accuracy of the SAR radial velocity.

The SAR imaging geometry is very important to the quality of the Doppler retrievals, particularly the surface velocity retrieval (Wang et al., 2014a). The satellite track angle for the descending ASAR image is about –13° (13° counterclockwise from north), which shows that the observed current direction is northwest–southeast. The satellite track angle for the ascending ASAR image is about –167°, corresponding to a northeast-southwest surface current direction. This direction is consistent with the central flow direction for the Kuroshio and KCC. The Kuroshio is orientated in the range direction for the ascending image, and its location corresponds to a high radar incidence angle. This makes the ASAR imaging geometry for the ascending track particularly appropriate for Doppler monitoring of the Kuroshio, and makes it suitable for capturing the spatial characteristics of the surface current.

In summary, surface radial current retrieved from SAR data using the Doppler centroid anomaly depends on the wavelength, incidence angle, and polarization mode of the radar instrument, and is modulated by sea surface winds, waves, and currents, which result in the SAR retrieved ocean current uncertainty. However, the Doppler frequency anomaly method represents a direct measure of sea surface current. So, it can provide an instantaneous and clear line-of-sight Doppler frequency shift. Also, it further confirms that the SAR scene contains quantitative ocean current information. The mean Doppler frequency shift of the ocean surface echo signal corresponds to a power-weighted mean line-of-sight velocity of the scatters (Romeiser and Thompson, 2000). Compared with the SAR backscatter coefficient, the Doppler frequency shift contains more sea state information, which can reveal the sea surface dynamics and explain some of the internal mechanisms of the sea surface motion. Therefore, the Doppler frequency can significantly complement SAR backscatter measurements and help to determine the quantitative relationship between complex surface roughness patterns and upper ocean dynamics. Moreover, Doppler frequency methods can be used to investigate mesoscale sea surface dynamics, SAR signal characteristics and local environmental conditions (Krug et al., 2010; Moiseev et al., 2020). These methods and findings presented here will be helpful for construction of an ocean current time-series, and it can provide boundary data to study formation and development mechanisms of the Kuroshio in the ECS.

5 Conclusions

In this work, we have used the theoretical model of Doppler frequency to estimate ocean surface current with a high spatial resolution from SAR data. We retrieved surface current properties from SAR data for the Kuroshio and the Kuroshio Counter Current and compared these with global ocean multi-observation products and global surface Lagrangian drifter data, showing that the radial current retrieved from SAR image scenes performs well. Our results show that radial current derived from SAR images can be used for monitoring ocean current velocities over a wide spatial area, at high spatial resolution and with high accuracy, and that the radial velocity appropriately represents surface flow dynamics. We analyzed uncertainties and sensitivities associated with the SAR radial current and found that complex surface wave motion and a strong NRCS gradient across the imaged scene can affect the accuracy of inversion calculations used to retrieve the current. The performance of the SAR in measuring radial current velocity acquired at radar incidence angles greater than 30° is closer to more directly *in-situ* observed current velocities and retrievals and these incidence angles are therefore more reliable. This research has developed our ability to map the central flow of the Kuroshio and the Kuroshio Counter Current. This study provides support for ocean current monitoring using SAR images, and for the construction of ocean current time-series from SAR data.

Acknowledgements

We acknowledge the data made available by the European Space Agency, the Copernicus Marine Service for the global ocean multi observation products and Drifter Data Assembly

Center for the global surface Lagrangian drifter data.

References

Ambe D, Imawaki S, Uchida H, et al. 2004. Estimating the Kuroshio axis south of Japan using combination of satellite altimetry and drifting buoys. Journal of Oceanography, 60(2): 375–382, doi: 10.1023/B:JOCE.0000038343.31468.fe

Chapron B, Collard F, Ardhuin F. 2005. Direct measurements of ocean surface velocity from space: Interpretation and validation. Journal of Geophysical Research: Oceans, 110(C7): C07008

Chapron B, Collard F, Kerbaol V. 2004. Satellite synthetic aperture radar sea surface Doppler measurements. In: Proceedings of the 2nd Workshop on Coastal and Marine Applications of SAR. Svalbard, Norway: ESA Special Publication

Deng Lijing, Wei Hao, Wang Jianing. 2015. Vertical distribution of the Kuroshio velocity in the Pollution Nagasaki section and its formative mechanism. Marine Science Bulletin, 17(1): 26–39

Essen H H, Gurgel K W, Schlick T. 2000. On the accuracy of current measurements by means of HF radar. IEEE Journal of Oceanic Engineering, 25(4): 472–480, doi: 10.1109/48.895354

European Space Agency. 2007. Envisat ASAR Product Handbook. European Space Agency. Issue 2.2. 218–559 https://earth.esa.int/eogateway/search?text=&categor=Document%20library&filter-envisat&subFiltr=product%20handbook [2007-02-27/2021-04-08]

Goldstein R M, Zebker H A, Barnett T P. 1989. Remote sensing of ocean currents. Science, 246(4935): 1282–1285, doi: 10.1126/science.246.4935.1282

Graber H C, Thompson D R, Carande R E. 1996. Ocean surface features and currents measured with synthetic aperture radar interferometry and HF radar. Journal of Geophysical Research: Oceans, 101(C11): 25813–25832, doi: 10.1029/96JC02241

Guan Bingxian. 1979. Some results from the study of the variation of the Kuroshio in the East China Sea. Oceanologia et Limnologia Sinica (in Chinese), 10(4): 297–306

Guo Xinyu, Miyazawa Y, Yamagata T. 2006. The Kuroshio onshore intrusion along the shelf break of the East China Sea: The origin of the Tsushima Warm Current. Journal of Physical Oceanography, 36(12): 2205–2231, doi: 10.1175/JPO2976.1

Han Shuzong, Yang Hua, Xue Wenhu, et al. 2017. The study of single station inverting the sea surface current by HF ground wave radar based on adjoint assimilation technology. Journal of Ocean University of China, 16(3): 383–388, doi: 10.1007/s11802-017-3189-8

Hansen M W, Collard F, Dagestad K F, et al. 2011a. Retrieval of sea surface range velocities from Envisat ASAR Doppler centroid measurements. IEEE Transactions on Geoscience and Remote Sensing, 49(10): 3582–3592, doi: 10.1109/TGRS.2011.2153864

Hansen M W, Johannessen J A, Dagestad K F, et al. 2011b. Monitoring the surface inflow of Atlantic Water to the Norwegian Sea using Envisat ASAR. Journal of Geophysical Research: Oceans, 116(C12): C12008, doi: 10.1029/2011JC007375

He Yijun. 2000. Ocean wave imaging mechanism by imaging radar. Science in China Series D: Earth Sciences, 43(6): 587–595, doi: 10.1007/BF02879502

He Yijun, Yang Xiaobo, Yi Na, et al. 2020. Progress in sea surface current retrieval from spaceborne SAR measurements. Journal of Nanjing University of Information Science and Technology (in Chinese), 12(2): 181–190

Jia Yongjun, Zhang Youguang, Lin Mingsen. 2013. The numerical simulation of the Kuroshio frontal eddies in the East China Sea using a hybrid coordinate ocean mode. Acta Oceanologica Sinica, 32(5): 31–41, doi: 10.1007/s13131-013-0311-7

Johannessen J A, Chapron B, Collard F, et al. 2008. Direct ocean surface velocity measurements from space: Improved quantitative interpretation of Envisat ASAR observations. Geophysical Research Letters, 35(22): L22608, doi: 10.1029/2008GL035709

Johannessen J A, Shuchman R A, Digranes G, et al. 1996. Coastal ocean fronts and eddies imaged with ERS 1 synthetic aperture radar. Journal of Geophysical Research: Oceans, 101(C3): 6651–6667, doi: 10.1029/95JC02962

Klemas V. 2012. Remote sensing of coastal and ocean currents: An overview. Journal of Coastal Research, 28(3): 576–586, doi: 10.2112/JCOASTRES-D-11-00197.1

Lehner S, Hoja D, Schulz-Stellenfleth J. 2002. Marine parameters from synergy of optical and radar satellite data. Advances in Space Research, 29(1): 23–32, doi: 10.1016/S0273-1177(01)00623-8

Li Shuiqing, Liu Baochang, Shen Hui, et al. 2020. Wind wave effects on remote sensing of sea surface currents from SAR. Journal of Geophysical Research: Oceans, 125(7): e2020JC016166

Lin Hui, Xu Qing, Zheng Quan'an. 2008. An overview on SAR measurements of sea surface wind. Progress in Natural Science, 18(8): 913–919, doi: 10.1016/j.pnsc.2008.03.008

Liu Baochang, He Yijun, Li Yongkang, et al. 2019. A new azimuth ambiguity suppression algorithm for surface current measurement in coastal waters and rivers with along-track InSAR. IEEE Transactions on Geoscience and Remote Sensing, 57(6): 3148–3165, doi: 10.1109/TGRS.2018.2881958

Ma Chao, Wu Dexing, Lin Xiaopei. 2009. Variability of surface velocity in the Kuroshio Current and adjacent waters derived from Argos drifter buoys and satellite altimeter data. Chinese Journal of Oceanology and Limnology, 27(2): 208–217, doi: 10.1007/s00343-009-9260-6

Moiseev A, Johnsen H, Hansen M W, et al. 2020. Evaluation of radial ocean surface currents derived from Sentinel-1 IW Doppler shift using coastal radar and Lagrangian surface drifter observations. Journal of Geophysical Research: Oceans, 125(4): e2019JC015743

Mouche A A, Collard F, Chapron B, et al. 2012. On the use of Doppler shift for sea surface wind retrieval from SAR. IEEE Transactions on Geoscience and Remote Sensing, 50(7): 2901–2909, doi: 10.1109/TGRS.2011.2174998

Qiu Bo, Chen Shuiming, Klein P, et al. 2020. Reconstructing upper-ocean vertical velocity field from sea surface height in the presence of unbalanced motion. Journal of Physical Oceanography, 50(1): 55–79, doi: 10.1175/JPO-D-19-0172.1

Qiu Bo, Lukas R. 1996. Seasonal and interannual variability of the North Equatorial Current, the Mindanao Current, and the Kuroshio along the Pacific western boundary. Journal of Geophysical Research: Oceans, 101(C5): 12315–12330, doi: 10.1029/95JC03204

Quilfen Y, Chapron B. 2019. Ocean surface wave-current signatures from satellite altimeter measurements. Geophysical Research Letters, 46(1): 253–261, doi: 10.1029/2018GL081029

Rio M H, Mulet S, Picot N. 2014. Beyond GOCE for the ocean circulation estimate: Synergetic use of altimetry, gravimetry, and in situ data provides new insight into geostrophic and Ekman currents. Geophysical Research Letters, 41(24): 8918–8925, doi: 10.1002/2014GL061773

Romeiser R. 2005. Current measurements by airborne along-track InSAR: Measuring technique and experimental results. IEEE Journal of Oceanic Engineering, 30(3): 552–569, doi: 10.1109/JOE.2005.857508

Romeiser R, Suchandt S, Runge H, et al. 2010. First analysis of TerraSAR-X along-track InSAR-Derived current fields. IEEE Transactions on Geoscience and Remote Sensing, 48(2): 820–829, doi: 10.1109/TGRS.2009.2030885

Romeiser R, Thompson D R. 2000. Numerical study on the along-track interferometric radar imaging mechanism of oceanic surface currents. IEEE Transactions on Geoscience and Remote Sensing, 38(1): 446–458, doi: 10.1109/36.823940

Krug M, Mouche A, Collard F, et al. 2010. Mapping the Agulhas Current from space: An assessment of ASAR surface current velocities. Journal of Geophysical Research: Oceans, 115(C10): C10026

Toporkov J V, Brown G S. 2000. Numerical simulations of scattering from time-varying, randomly rough surfaces. IEEE Transactions on Geoscience and Remote Sensing, 38(4): 1616–1625, doi: 10.1109/36.851961

Wang Lihua, Zhou Yunxuan, Ge Jianzhong, et al. 2014a. Mapping sea surface velocities in the Changjiang coastal zone with advanced synthetic aperture radar. Acta Oceanologica Sinica,

33(11): 141–149, doi: 10.1007/s13131-014-0563-x

Wang Lihua, Zhou Yunxuan, Zhu Jianrong, et al. 2014b. Deriving Changjiang coastal zone wind from C-band SAR and its application to salinity simulation. Chinese Journal of Oceanology and Limnology, 32(4): 946–957, doi: 10.1007/s00343-014-3253-9

Yoshida T, Rheem C K. 2015. Time-domain simulation of along-track interferometric SAR for moving ocean surfaces. Sensors, 15(6): 13644–13659, doi: 10.3390/s150613644

Zhang Canying, Feng Zhigang, Zhang Xiaokun, et al. 2017. Analysis on research progress of Kuroshio. World Sci-Tech R&D (in Chinese), 39(3): 239–249

Zhuang Zhanpeng, Hui Zhenli, Yang Guangbing, et al. 2020. Principal-component estimates of the Kuroshio Current axis and path based on the mathematical verification between satellite altimeter and drifting buoy data. Acta Oceanologica Sinica, 39(1): 14–24, doi: 10.1007/s13131-019-1523-2